Divergence of acetate uptake in proinflammatory and inflammation-resolving macrophages: implications for imaging atherosclerosis

Selim Demirdelen, MD,[a] Philip Z. Mannes,[a] Ali Mubin Aral, MD,[a] Joseph Haddad, MD,[a] Steven A. Leers, MD,[b] Delphine Gomez, PhD,[c,d] and Sina Tavakoli, MD, PhD[a,c,d,e]

[a] Department of Radiology, University of Pittsburgh, Pittsburgh, PA
[b] Department of Surgery, University of Pittsburgh, Pittsburgh, PA
[c] Department of Medicine, University of Pittsburgh, Pittsburgh, PA
[d] Heart, Lung, Blood, and Vascular Medicine Institute, UPMC Department of Medicine, Pittsburgh, PA
[e] UPMC Presbyterian Hospital, Pittsburgh, PA

Received Apr 2, 2020; accepted Dec 1, 2020
doi:10.1007/s12350-020-02479-5

Background. **Metabolic divergence of macrophages polarized into different phenotypes represents a mechanistically relevant target for non-invasive characterization of atherosclerotic plaques using positron emission tomography (PET). Carbon-11 (^{11}C)-labeled acetate is a clinically available tracer which accumulates in atherosclerotic plaques, but its biological and clinical correlates in atherosclerosis are undefined.**

Methods and results. **Histological correlates of ^{14}C-acetate uptake were determined in brachiocephalic arteries of western diet-fed apoE$^{-/-}$ mice. The effect of polarizing stimuli on ^{14}C-acetate uptake was determined by proinflammatory (interferon-γ + lipopolysaccharide) vs inflammation-resolving (interleukin-4) stimulation of murine macrophages and human carotid endarterectomy specimens over 2 days. ^{14}C-acetate accumulated in atherosclerotic regions of arteries. CD68-positive monocytes/macrophages vs smooth muscle actin-positive smooth muscle cells were the dominant cells in regions with high vs low ^{14}C-acetate uptake. ^{14}C-acetate uptake progressively decreased in proinflammatory macrophages to 25.9 ± 4.5% of baseline ($P < .001$). A delayed increase in ^{14}C-acetate uptake was induced in inflammation-resolving macrophages, reaching to 164.1 ± 21.4% ($P < .01$) of baseline. Consistently, stimulation of endarterectomy specimens with interferon-γ + lipopolysaccharide decreased ^{14}C-acetate uptake to 66.5 ± 14.5%, while interleukin-4 increased ^{14}C-acetate uptake to 151.5 ± 25.8% compared to non-stimulated plaques ($P < .05$).**

The authors of this article have provided a PowerPoint file, available for download at SpringerLink, which summarizes the contents of the paper and is free for re-use at meetings and presentations. Search for the article DOI on SpringerLink.com.

The authors have also provided an audio summary of the article, which is available to download as ESM, or to listen to via the JNC/ASNC Podcast.

Electronic supplementary material The online version of this article (https://doi.org/10.1007/s12350-020-02479-5) contains supplementary material, which is available to authorized users.

Funding This study was supported by grants from National Institutes of Health (NHLBI, K08 HL144911) and Radiological Society of North America (RSD-1820), and a Seed Fund from University of Pittsburgh/UPMC Departments of Radiology and Medicine to S.T; as well as a grant from National Institutes of Health (NHLBI R01 HL146465) to D.G.

Reprint requests: Sina Tavakoli, MD, PhD, UPMC Presbyterian Hospital, 200 Lothrop Street, Suite E200, Pittsburgh, PA 15213; *sit23@pitt.edu*

1071-3581/$34.00

Conclusions. **Acetate uptake by macrophages diverges upon proinflammatory and inflammation-resolving stimulation, which may be exploited for immunometabolic characterization of atherosclerosis. (J Nucl Cardiol 2022;29:1266–76.)**

Key Words: Acetate • atherosclerosis • macrophage polarization • metabolism • imaging

Abbreviations	
^{18}F-FDG	^{18}F-fluorodeoxyglucose
PET	Positron emission tomography
IL-1β	Interleukin-1β
IL-4	Interleukin-4
IFN-γ	Interferon-γ
LPS	Lipopolysaccharide
NOS2	Nitric oxide synthase-2

See related editorial, pp. 1277–1279

INTRODUCTION

Immunometabolism, i.e., the cross-talk of intracellular metabolic pathways and immune cell function, plays a pivotal role in the pathogenesis of inflammatory diseases, including atherosclerosis.[1–3] For example, hypoxia, a major trigger of enhanced glycolysis in atherosclerotic plaques, promotes the production of proinflammatory cytokines, e.g., interleukin-1β, by macrophages,[4–6] and expansion of the necrotic core.[7] Moreover, proinflammatory stimulation of macrophages by lipopolysaccharide (LPS) enhances glucose uptake and glycolysis,[8–10] which in turn accentuates the production of interleukin-1β through succinate-mediated stabilization of hypoxia-inducible factor-1α and development of a pseudo-hypoxic state.[8] The unprecedented recognition of the vessel wall immunometabolic heterogeneity and its mechanistic contribution to atherogenesis provides the opportunity to explore the potential applications of metabolic imaging in cardiovascular diseases, analogous to similar efforts in oncology.[11,12]

Imaging of glucose utilization by ^{18}F-fluorodeoxyglucose (^{18}F-FDG) positron emission tomography (PET) has been instrumental in elucidating the in vivo metabolic heterogeneity of the vessel wall, supplementing the information obtained by ex vivo metabolomics techniques.[1] However, the non-specificity of ^{18}F-FDG uptake, which targets a nearly ubiquitous metabolic process upregulated in both proinflammatory and inflammation-resolving (reparative) states, makes it suboptimal for characterization of the inflammatory response as a stand-alone imaging marker.[9,10,13–15] Additionally, myocardial uptake of ^{18}F-FDG has been a major challenge for its utilization in coronary artery disease.[15,16] These limitations have prompted investigators to exploit the utility of metabolic substrates other than glucose, e.g., glutamine[9] and acetate,[17,18] in non-invasive characterization of plaque immunometabolism. Notably, the safety of several metabolic substrates has already been established in oncological or cardiac imaging studies,[17,19] which facilitates their applications in imaging atherosclerosis.

Carbon-11 (^{11}C)-labeled acetate (^{11}C-acetate) has been extensively studied to detect cancer-associated lipogenesis and myocardial blood flow and oxidative metabolism.[20,21] More recently, pre-clinical[18] and pilot clinical[17] studies have demonstrated the feasibility of imaging ^{11}C-acetate uptake in atherosclerosis. However, the biological correlates of acetate uptake in plaques and its clinical implications have not been addressed. The purpose of this study was to determine the histological correlates of acetate uptake in atherosclerotic plaques and its link to inflammatory states of macrophages, using ^{14}C-acetate where the long half-lived β-emitting C-14 allows for ex vivo imaging via autoradiography. We hypothesized that acetate uptake in macrophage-rich plaques differentiates their proinflammatory vs inflammation-resolving polarization states. Histological correlates of acetate uptake were determined by combined immuno-histology and high-resolution ^{14}C-acetate autoradiography in murine atherosclerotic brachiocephalic arteries. The effect of proinflammatory vs inflammation-resolving stimuli on acetate uptake was assessed in murine macrophage and human carotid endarterectomy specimens.

MATERIALS AND METHODS

Animals

Wild-type (N = 12) and apoE$^{-/-}$ (N = 3) mice on a C57BL/6J background were purchased from Jackson Laboratories. Atherosclerosis was induced by feeding with a western diet (21% anhydrous fat, TD88137, Envigo, 33 weeks) in apoE$^{-/-}$ mice. Experiments were conducted in accordance with a protocol approved by Institutional Animal Care and Use Committee.

Cell Culture

Commercial experimental reagents are listed in Supplemental Table 1. Elicited peritoneal cells were harvested from wild-type mice through lavage, three days after intra-peritoneal injection of 1.5 mL of 3% thioglycolate.[22] Adherent macrophages were cultured for 2 days in RPMI-1640 supplemented with 10% fetal bovine serum, glucose (5.5 mM), sodium pyruvate (1 mM), glutamine (2 mM), non-essential amino acids (1 ×), HEPES buffer (20 mM), penicillin (50 U·mL^{-1}), and streptomycin (50

$\mu g \cdot mL^{-1}$), as described.[9,10,13] Macrophages which were not activated by the addition of polarizing stimuli were considered as non-activated ($M\varphi_0$). Polarization was induced by addition of the conventional proinflammatory (M1) or inflammation-resolving (M2) stimuli: (i) $M\varphi_{IFN\gamma + LPS}$: recombinant murine interferon-γ (50 $ng \cdot mL^{-1}$) plus LPS (10 $ng \cdot mL^{-1}$) and (ii) $M\varphi_{IL4}$: recombinant murine IL-4 (10 $ng \cdot mL^{-1}$).

Primary aortic vascular smooth muscle cells (VSMCs) obtained from C57BL/6J mice[23] were cultured for 2 days in DMEM/F12 supplemented with 10% fetal bovine serum, L-glutamine (2 mM), HEPES buffer (10 mM), penicillin (100 $U \cdot mL^{-1}$), and streptomycin (100 $\mu g \cdot mL^{-1}$). Polarization was induced by addition of the conventional proinflammatory or inflammation-resolving stimuli: (i) $VSMC_{IFN\gamma + LPS}$: recombinant murine interferon-γ (50 $ng \cdot mL^{-1}$) plus LPS (10 $ng \cdot mL^{-1}$) and (ii) $VSMC_{IL4}$: recombinant murine IL-4 (10 $ng \cdot mL^{-1}$).

Culture of Human Endarterectomy Specimens

Anonymized atherosclerotic specimens were collected from three patients who underwent carotid endarterectomy as the standard-of-care, under a ''No Human Subject involvement'' classification by Institutional Review Board. Freshly collected specimens were cut into $\sim$ 3-mm thick slices and cultured ex vivo in complete RPMI-1640 medium.[24,25] Plaques were incubated for two days in the absence (control) or presence of (i) recombinant human interferon-γ (50 $ng \cdot mL^{-1}$) plus LPS (10 $ng \cdot mL^{-1}$) vs (ii) recombinant human IL-4 (10 $ng \cdot mL^{-1}$).

Uptake of ^{14}C-Acetate by Macrophages and VSMCs

^{14}C-acetate uptake was measured in macrophages and VSMCs after 6, 24 or 48 hours of polarization. Immediately prior to the assay, cells were washed with phosphate-buffered saline and were incubated with an uptake buffer (NaCl 140 mM, KCl 5.4 mM, $CaCl_2$ 1.8 mM, $MgSO_4$ 0.8 mM, D-glucose 5.5 mM, HEPES 25 mM) supplemented with 2 $\mu Ci \cdot mL^{-1}$ (74 $kBq \cdot mL^{-1}$) ^{14}C-acetate at 37 °C for 2 hours. Subsequently, cells were washed and lysed with 0.1 mM NaOH. ^{14}C-acetate uptake was quantified by a liquid scintillation counter (Beckman Coulter LS6500), normalized to the DNA content of the cell lysates (PicoGreen, Invitrogen), and expressed relative to the uptake values of unstimulated $M\Phi_0$ or VSMCs.[9,10,13]

Micro-autoradiography of ^{14}C-Acetate Uptake

Excised murine brachiocephalic arteries or human endarterectomy specimens were incubated with the uptake buffer (described above) supplemented with 2 $\mu Ci \cdot mL^{-1}$ (74 $kBq \cdot mL^{-1}$) ^{14}C-acetate at 37 °C for 2 hours. Specimens were then washed with a cold buffer and embedded in optimal cutting temperature (OCT) compound for cryosectioning (Leica CM1860) at 10 μm thickness. Tissues, along with known amounts of ^{14}C-acetate blotted on papers as standards, were exposed to high-resolution phosphor screens (BAS-IP SR2025 Super Resolution, GE Healthcare). Phosphor screens were scanned by a Sapphire Biomolecular Imager (Azure Biosystems) at 10-μm resolution. Autoradiography images were adjusted using the Fire Look-Up Table and a smoothing algorithm (ImageJ). The average uptake of ^{14}C-acetate by endarterectomy specimens stimulated with proinflammatory and inflammation-resolving stimuli was quantified (ImageJ) by drawing regions of interests around the tissues (2-3 sections per specimen at 250 μm intervals). Uptake values are expressed relative to control (non-stimulated) plaques.

Histology

Histological analysis of the brachiocephalic arteries was performed after completion of the autoradiography by Movat's pentachrome staining per standard protocols. Smooth muscle cells and macrophages were identified by immunostaining with anti-mouse α-smooth muscle actin (αSMA) and anti-mouse CD68, respectively (Supplemental Table 1). Immunostaining for inducible nitric oxide synthase (iNOS) and CD206 was performed as conventional markers of M1 and M2 polarization, respectively. Slides were mounted using ProLong™ Gold Antifade with 4′,6-diamidino-2-phenylindole (DAPI) for nuclear counter-staining. Tissues were photographed using an AxioVert Microscope (Zeiss) equipped with a digital camera, controlled by ZEN software (Zeiss).

High-Resolution Quantification of ^{14}C-Acetate Uptake

AzureSpot software was used to place a 5 × 5 μm grid on top of overlayed autoradiography and immunostaining (both CD68 and αSMA) (Supplemental Figure 1). ^{14}C-acetate intensity data were transferred to FlowJo 10.5.3 software. Each 5 × 5 μm box was ranked from the lowest to the highest based on its ^{14}C-acetate uptake and assigned a quartile (Q1 = lowest, Q4 = highest). $CD68^+$ and αSMA^+ percent areas were determined in each quartile of ^{14}C-acetate uptake (averaged from 2 to 3 tissues sections per mouse).

Gene Expression Analysis

Messenger RNA (mRNA) extraction and reverse transcription were performed on cultured mouse macrophages and endarterectomy specimens 2 days after stimulation using TRIzol® reagent and QuantiTect® Reverse Transcription Kit, per standard protocols.[9,10,13] Quantitative PCR (qPCR) was performed using a QuantStudio-3 Real-Time PCR System (ThermoFisher) and TaqMan® gene expression assays (Supplemental Table 2). Transcript amplification data were analyzed using QuantStudio v1.4.3 software (Applied Biosystems) and were normalized to the expression level of 18S ribosomal RNA (*Rn18s*), as the housekeeping gene. mRNA expression levels are expressed as relative to the level of

expression in Mφ_0 macrophages and summarized as a heat map. Transcript levels of macrophage polarization markers in endarterectomies are expressed relative to the expression of CD68 to account for variations in the macrophage contents of different specimens.

Statistical Analysis

Data were expressed as mean ± standard error of the mean. Statistical analyses were performed with Prism-8 software (GraphPad). Student *t* test or analysis of variance (followed by Fisher's exact post hoc test) was used to test the differences between two or multiple groups, respectively. $P < .05$ was considered statistically significant.

RESULTS

Uptake of ^{14}C-Acetate by Macrophage-Rich Murine Brachiocephalic Artery Plaques

Micro-autoradiography of murine brachiocephalic arteries from western diet-fed apoE$^{-/-}$ mice demonstrated focal areas of increased ^{14}C-acetate uptake in the vessel wall, corresponding to atherosclerotic plaques, as confirmed by overlaid histological (Movat's pentachrome staining) and autoradiography images (Figure 1A). Consistent with the visual assessment, quantitative assessment of the brachiocephalic arteries trended towards higher ^{14}C-acetate uptake in plaques compared to plaque-free regions (Figure 1B). To determine the cellular composition of plaque regions with focal ^{14}C-acetate uptake, we performed immunofluorescent staining of brachiocephalic arteries using CD68 and αSMA antibodies, delineating macrophages and smooth muscle cells, as the two most abundant cells within the plaques. As demonstrated in representative images of combined autoradiography and immunostaining (Figures 2A-D), CD68$^+$ macrophages were highly abundant in plaque regions with high ^{14}C-acetate uptake. Quantification of CD68$^+$ and αSMA$^+$ areas (Figure 2E) confirmed that macrophages were the predominant cells in regions with the highest quartile (Q4) of ^{14}C-acetate uptake (CD68$^+$ macrophages: 41.2 ± 0.8% vs αSMA$^+$ smooth muscle cells: 18.1 ± 3.5%, $P < .01$). On the other hand, vessel wall regions with the lowest quartile (Q1) of ^{14}C-acetate uptake were predominantly comprised of αSMA$^+$ smooth muscle cells (43.3 ± 1.3%) compared with CD68$^+$ macrophages (30.5 ± 2.1%) (Figure 2E, $P < .01$). Of note, ^{14}C-acetate uptake within the macrophage-rich regions of plaques was heterogeneous, and CD68$^+$ regions consisted of areas with high (marked by the red oval shape in Figures 2A and D) and low (marked by the red box in Figures 2A and D) ^{14}C-acetate uptake. On the other hand, smooth muscle cells both within the plaques (blue arrows in Figures 2B and D) and normal regions of arteries (blue arrowheads in Figures 2B and D) had relatively low ^{14}C-acetate uptake.

Divergence of ^{14}C-Acetate Uptake upon M1 and M2 Polarization of Macrophages

The striking heterogeneity of ^{14}C-acetate uptake in CD68$^+$ regions of plaques led us to examine the association between acetate uptake and different polarization states of macrophages. We determined through immunofluorescence staining that both M1-like (CD68$^+$/iNOS$^+$) and M2-like (CD68$^+$/CD206$^+$) macrophages were present in murine brachiocephalic plaque (Supplemental Figure 2).

We utilized a conventional approach to induce proinflammatory (M1) and inflammation-resolving (M2) polarization states in murine macrophages using IFN-γ

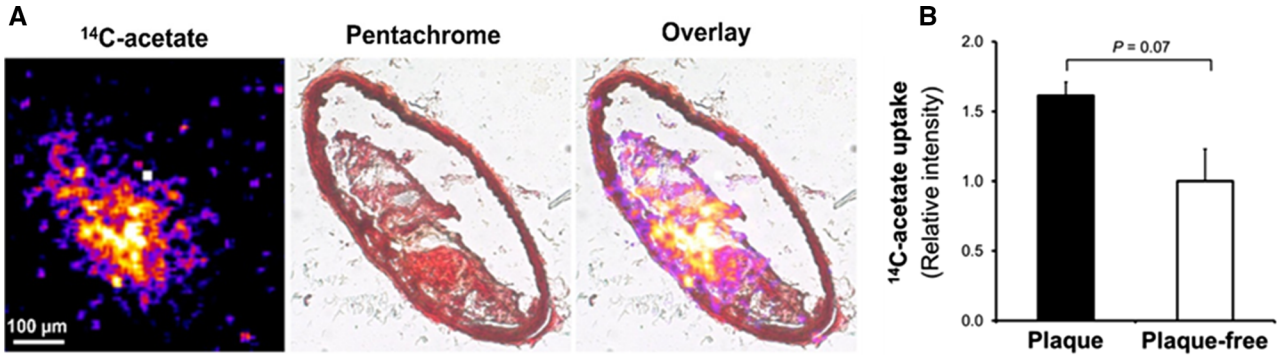

Figure 1. Focal uptake of ^{14}C-acetate by murine atherosclerotic plaques. Micro-autoradiography (**A**, left), Movat's pentachrome (**A**, middle), and their superimposed (**A**, right) images demonstrate that vessel wall ^{14}C-acetate uptake colocalizes with brachiocephalic artery atherosclerotic plaques of apoE$^{-/-}$ mice fed with a western diet. Plaque uptake of ^{14}C-acetate (**B**) trended higher in arterial regions with plaques rather than plaque-free regions.

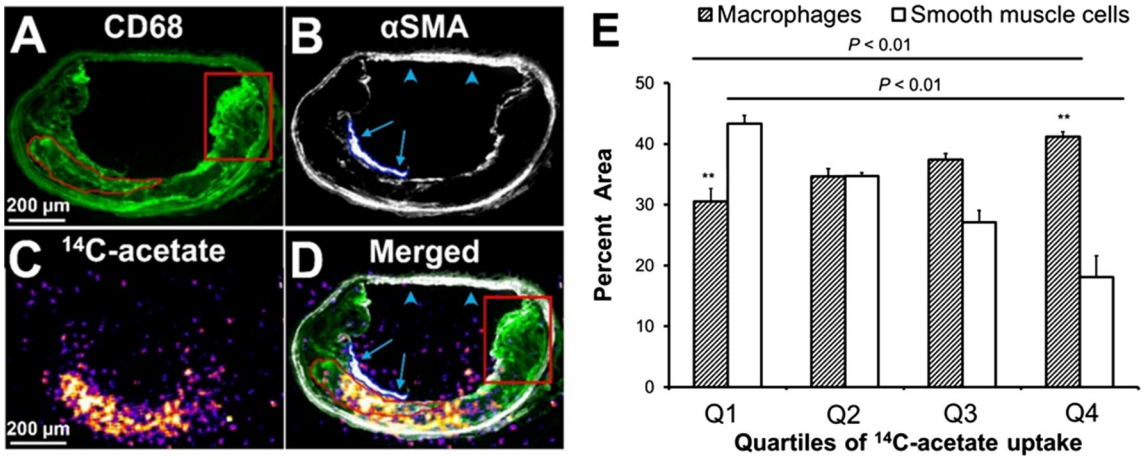

Figure 2. Colocalization of ^{14}C-acetate uptake and macrophage-rich regions of atherosclerotic plaques. Combined micro-autoradiography and immunofluorescent staining for CD68 (macrophage marker) and αSMA (smooth muscle cell marker) (**A**-**D**) demonstrates that areas of focal uptake of ^{14}C-acetate primarily correspond to macrophage-rich regions of murine brachiocephalic artery atherosclerotic plaques. Of note, ^{14}C-acetate uptake within the macrophage-rich regions of plaques was heterogeneous. Some macrophage-rich regions demonstrated high ^{14}C-acetate uptake (marked by the red oval shape in **A** and **D**), while other regions had low uptake (marked by the red box in **A** and **D**). Smooth muscle cells both within the plaque (blue arrows in **B** and **D**) and normal regions of artery (blue arrowheads in **B** and **D**) had relatively low ^{14}C-acetate uptake. Quantification of CD68$^+$ and αSMA$^+$ areas in vessel wall regions with increasing quartiles of ^{14}C-acetate uptake (**E**) confirms that macrophages are the most abundant cells in regions with higher ^{14}C-acetate uptake, while smooth muscle cells comprise the most abundant cells in regions with lower ^{14}C-acetate uptake (N = 3 mice, 2-3 tissue sections per each mouse). **indicates $P < .01$ for within quartile comparison of abundance of macrophages and VSMCs; P values above the brackets indicates between quartiles comparisons of the abundance of macrophages and VSMCs.

plus LPS ($M\varphi_{IFN\gamma + LPS}$) and IL-4 ($M\varphi_{IL4}$), respectively, over a 2-day period. Successful conversion of macrophages into different polarization states was confirmed by markedly different transcript levels of a panel of conventional M1 (*Arg2*, *Cxcl9*, *Cxcl10*, *Il1b*, *Nos2*, and *Tnf*) and M2 (*Arg1*, *Cd36*, *Chil3*, *Mrc1*, *Tfrc*, *Tgfb*) markers (Figure 3).

The uptake of ^{14}C-acetate by macrophages was determined at 6, 24, and 48 hours after the induction of polarization. As demonstrated in Figure 4A, there was a steady decline in ^{14}C-acetate uptake in $M\varphi_{IFN\gamma + LPS}$, which was noticeable as early as 6 hours after stimulation (59.5 ± 3.7% of the baseline level, $P < .001$) and reached to its minimum at 48 hours (25.9 ± 4.5% of the baseline level, $P < .001$). On the other hand, $M\varphi_{IL4}$ demonstrated a significant, but delayed, increase in ^{14}C-acetate uptake, reaching to 164.1 ± 21.4% of the baseline level at 48 hours after stimulation ($P < .01$). The ^{14}C-acetate uptake by VSMCs, however, was essentially unchanged upon stimulation by either IFN-γ + LPS or IL-4 (Supplemental Figure 3).

The transport of acetate through cell membrane occurs through members of the monocarboxylate transporter family.[26] Therefore, we determined the mRNA expression of *Slc16a1*, *Slc6a3*, and *Slc16a7*, encoding monocarboxylic acid transporter-1, -3, and -2, respectively (Figures 4B-D). The expression of *Slc16a1*, representing the most abundant of the three transporters,[26,27] was 3.9 ± 0.3 ($P = .05$) and 6.3 ± 1.6 ($P < .01$)-fold higher in $M\varphi_{IFN\gamma + LPS}$ and $M\varphi_{IL4}$ compared to $M\varphi_0$, respectively ($P < .001$). The expression of *Slc16a3* was also 6.1 ± 1.3 ($P < .01$) and 3.3 ± 1.2 ($P = .14$)-fold higher in $M\varphi_{IFN\gamma + LPS}$ and $M\varphi_{IL4}$ compared to $M\varphi_0$, respectively. The expression of *Slc16a7*, the least abundant transporter, was comparable among the different polarization states of macrophages.

^{14}C-Acetate Uptake by Human Carotid Plaques Stimulated by IFN-γ + LPS vs IL-4 Mirrors the Changes in Polarized Macrophages

In order to determine the effect of different polarizing agents on acetate uptake in the vessel wall microenvironment, we utilized a previously validated technique of ex vivo culture of human carotid endarterectomy specimens.[24,25] Induction of different polarization states in endarterectomy specimens was

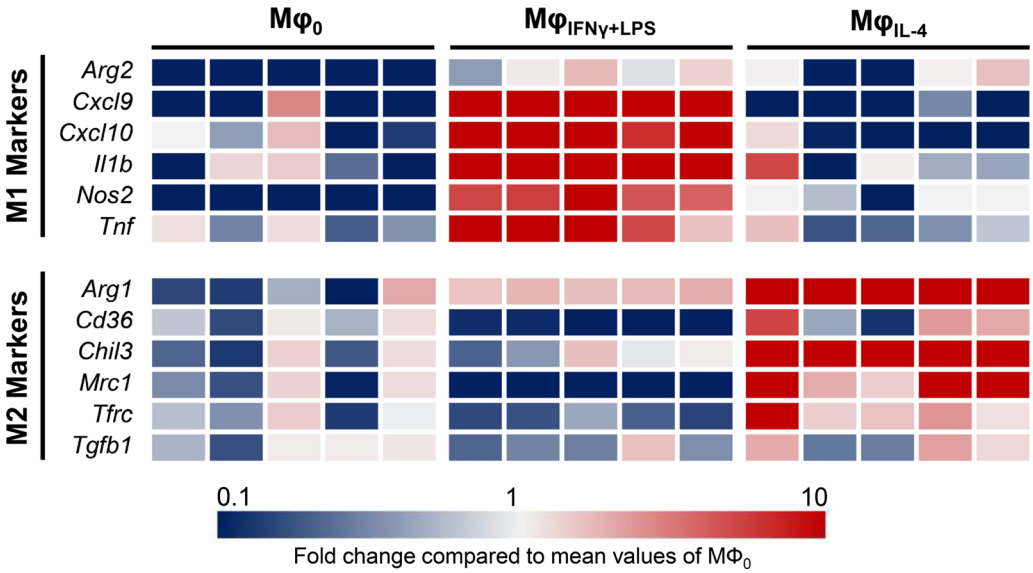

Figure 3. Distinct inflammatory profiles of Mφ_0, M$\varphi_{IFN\gamma + LPS}$ and Mφ_{IL4}. Heat map illustration of macrophage polarization transcript levels (relative to Mφ_0) confirms the development of distinct polarization phenotypes upon 2-day culture of murine macrophages with by IFN-γ + LPS vs IL-4 (N = 5).

confirmed by the increased expression of M1 polarization markers, interleukin-1β (IL-1β) and nitric oxide synthase-2 (NOS2), by IFN-γ + LPS (Figure 5A) vs M2 polarization markers, CD163 and mannose receptor C-type 1 (MRC1), by IL-4 (Figure 5B). Consistent with our observation in polarized murine macrophages, stimulation of human endarterectomy specimens with IFN-γ + LPS led to reduction of ^{14}C-acetate uptake to 66.5 ± 14.5% of non-stimulated plaques over a 2-day period (Figures 5C and D). On the other hand, stimulation by IL-4 increased ^{14}C-acetate uptake to 151.5 ± 25.8% (Figures 5C and D) ($P < .05$).

DISCUSSION

As summarized in schematic Figure 6, our study demonstrated that uptake of acetate is primarily localized to macrophage-rich regions of atherosclerotic plaques. Additionally, we showed a divergence in acetate uptake by macrophages and endarterectomy specimens stimulated with proinflammatory (IFN-γ + LPS) vs inflammation-resolving (IL-4) stimuli, suggesting the potential of ^{11}C-acetate PET in characterizing the inflammatory state of the vessel wall.

The growing appreciation of the contribution of plaques' immunometabolic heterogeneity to the vessel wall biology[1] underscores the potential role of metabolic imaging in non-invasive characterization of atherosclerosis, which may improve the risk stratification of patients and monitoring the response to preventive or therapeutic interventions.[15,16] To further enhance the translational potential of this study, we used murine brachiocephalic plaques, rather than aortic plaques, as the former more accurately models the complexities of human plaque pathophysiology.[28–30]

Despite initial promising results indicating an association between ^{18}F-FDG uptake and the proinflammatory state of vessel wall macrophages,[15,16,31] emerging evidence supports that glucose uptake, as a stand-alone marker, does not reveal sufficient immunometabolic information to allow discrimination of plaques macrophages from smooth muscle cells[14,32] or proinflammatory from inflammation-resolving macrophages.[5,9,10,13]

A promising approach to overcome the non-specificity of ^{18}F-FDG in elucidating vessel wall immunometabolism is a combined imaging approach to target other key metabolic pathways, which may aid in differentiation of different immune cell phenotypes. For example, combined imaging of glutamine and glucose uptake improves the identification of different polarization states of macrophages.[9] Considering the central roles of acetate in various immunometabolic pathways, including tricarboxylic acid cycle, lipogenesis, and protein acetylation,[33] ^{11}C-acetate PET represents a promising, but largely unexplored, approach in inflammatory diseases. Notably, ^{11}C-acetate uptake has been reported in ∼ 30% of atherosclerotic

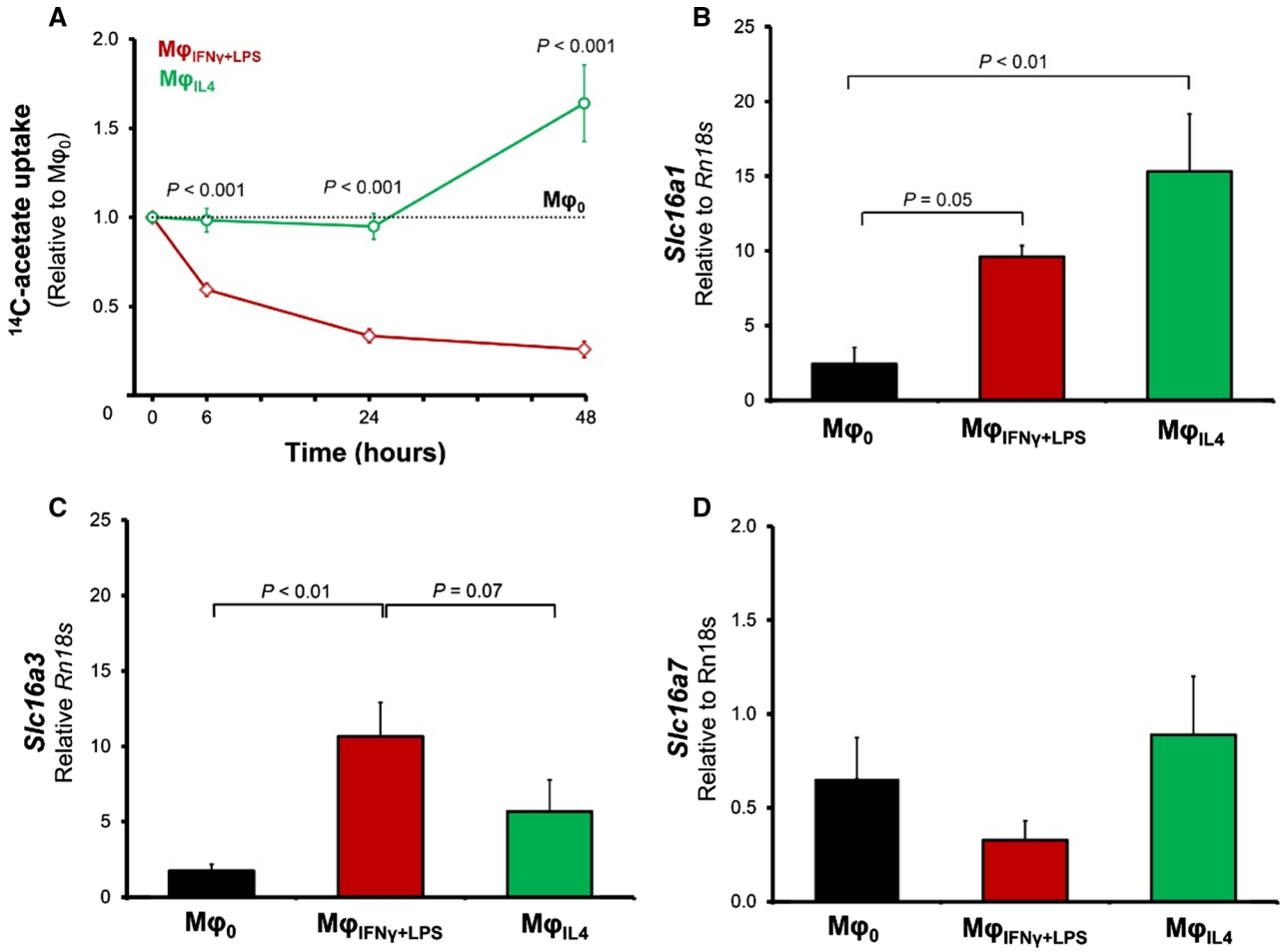

Figure 4. Divergence of ^{14}C-acetate uptake in M$\varphi_{IFN\gamma + LPS}$ and Mφ_{IL4}. Stimulation of murine macrophages with IFN-γ + LPS vs IL-4 resulted in the divergence of ^{14}C-acetate uptake (**A**), characterized by a progressive decline by ~ 4-folds in M$\varphi_{IFN\gamma + LPS}$ and a delayed ~ 64% increase in Mφ_{IL4}. mRNA level of *Slc16a1* (**B**) is increased in both M$\varphi_{IFN\gamma + LPS}$ (3.9-fold) and Mφ_{IL4} (6.3-fold). Expression of *Slc16a3* transcript (**C**) was also increased in M$\varphi_{IFN\gamma + LPS}$ (6.1-fold); but the apparent overexpression of *Slc16a3* in Mφ_{IL4} (3.3-fold) did not reach statistical significance (P = .14). The expression of *Slc16a7* (**D**) was not significantly changed by the polarization state of macrophages (N = 7 for uptake assays and = 5 for gene expression assays).

plaques.[17] However, biological/immunometabolic correlates and clinical implications of acetate uptake in atherosclerosis remained to be determined. In this study, we showed that acetate uptake is primarily localized to macrophage-rich regions of atherosclerosis.

In order to identify the immunometabolic implications of acetate uptake, we determined the time-course of changes in cultured macrophages over a 2-day period of ex vivo polarization. We identified a progressive decline in acetate uptake by proinflammatory macrophages, but a delayed increase in acetate uptake in inflammation-resolving macrophages. The distinct temporal pattern of acetate uptake in polarized macrophages may reflect differences in IFN-γ + LPS vs IL-4-induced cellular metabolic reprogramming, particularly in M2-like macrophages which rely on mitochondrial biogenesis for activation and subsequent upregulation of specific metabolic pathways (e.g., tricarboxylic acid cycle, β-oxidation, oxidative phosphorylation).[10,34,35] By contrast, IFN-γ + LPS stimulation affects macrophage metabolism by more rapid regulation of flux through certain pathways, including enhanced glycolysis and suppression of the tricarboxylic acid cycle and oxidative phosphorylation cycle.[8] This divergence of acetate uptake in differentially polarized macrophages highlights the potential role of ^{11}C-acetate PET in non-invasive discrimination of inflammatory states of atherosclerotic plaques. As a proof-of-principle ex vivo

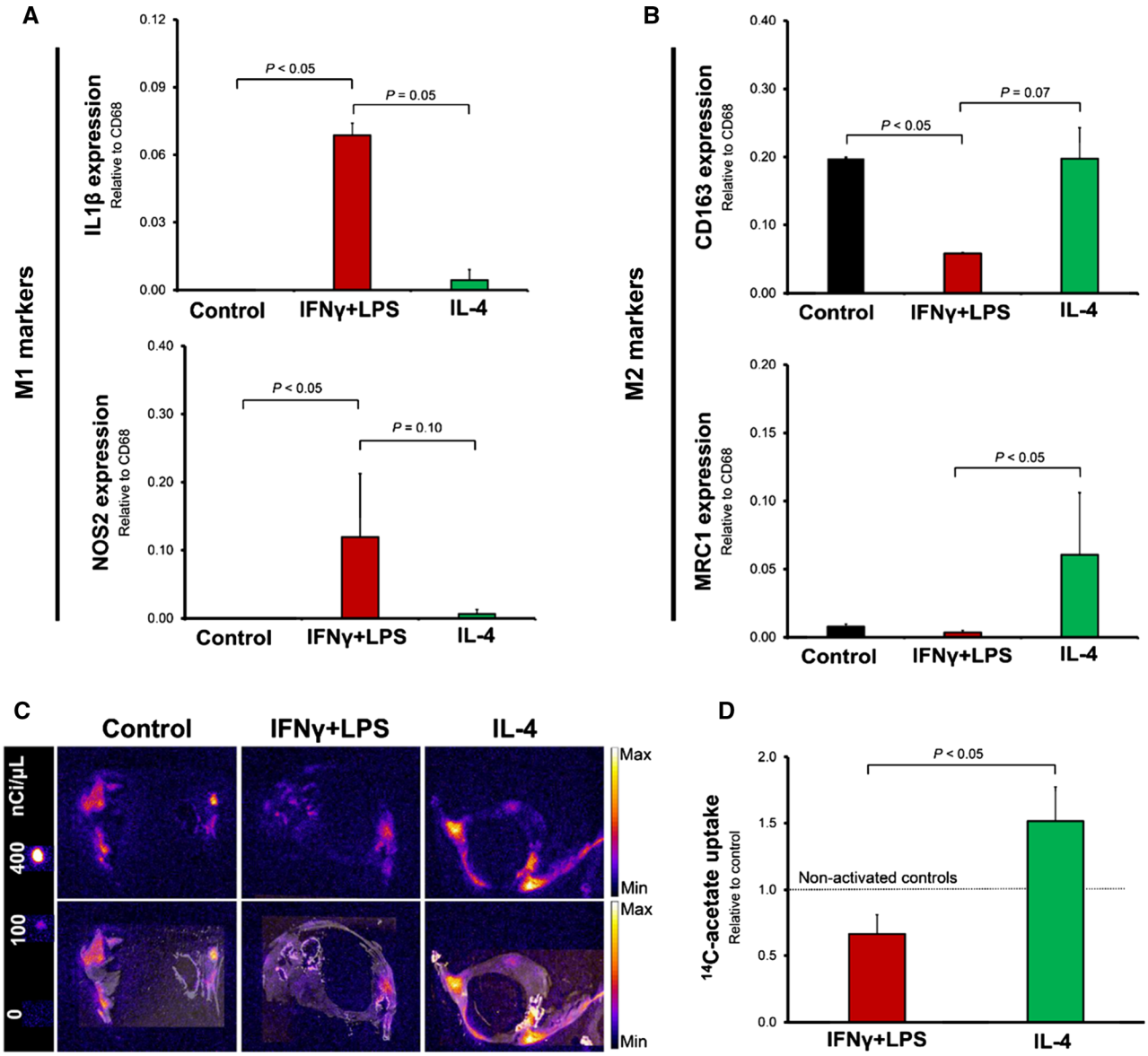

Figure 5. Divergence of ^{14}C-acetate uptake by human atherosclerotic plaques upon proinflammatory vs inflammation-resolving stimulation. Induction of distinct polarization states in human carotid endarterectomy specimens is confirmed by quantification of M1 polarization markers [interleukin-1β (IL-1β) and nitric oxide synthase-2 (NOS2), panel **A**] vs M2 polarization markers [CD163 and mannose receptor C-type 1 (MRC1), panel **B**]. Quantitative autoradiography demonstrates that stimulation of plaques with IFN-γ + LPS leads to a significant decline in ^{14}C-acetate uptake, while IL-4 stimulation increases ^{14}C-acetate uptake (**C**-**D**). N = 3 endarterectomy specimens (2-3 tissue sections per each specimen quantified).

experiment, we confirmed that IFN-γ + LPS reduces, while IL-4 increases, the acetate uptake in human endarterectomy specimens.

Cellular transport of acetate is primarily through monocarboxylate transporters.[26] Consistent with prior reports, *Slc16a1* and *Slc16a3* were the most abundant transporters at the transcriptional level.[26,27] Interestingly, *Slc16a1* was ~ 6-fold over-expressed in Mφ_{IL4}, consistent with their higher acetate uptake, compared to Mφ_0. There was also ~ 4- and ~ 6-fold increase in the expression of *Slc16a1* and *Slc16a3* in M$\varphi_{IFN\gamma + LPS}$, despite their markedly reduced acetate uptake, which likely reflects their role in transport of other substrates, particularly lactate, which is required

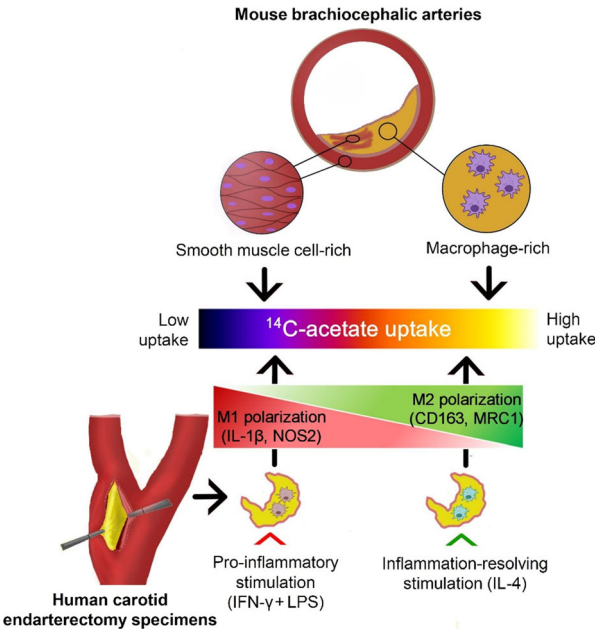

Figure 6. Schematic summary of the study. ^{14}C-acetate uptake is primarily localized within the macrophage-rich regions of atherosclerotic plaques in brachiocephalic arteries of apoE$^{-/-}$ mice. Ex vivo polarization of murine peritoneal macrophages and human carotid endarterectomy specimens into proinflammatory and inflammation-resolving states, by IFN-γ + LPS vs IL-4, respectively, leads to a marked divergence in their uptake of ^{14}C-acetate, suggesting a potential avenue for immunometabolic characterization of atherosclerotic plaques by PET.

for glycolytic reprogramming of macrophages in response to LPS.[36]

Intra-cellular metabolic fate of various substrates, e.g., glucose and glutamine, plays crucial role in phenotypic alterations of macrophages in response to different stimuli.[8,37–39] Through acetyl-CoA synthetase-mediated conversion into acetyl-CoA and subsequent condensation with oxaloacetate to generate citrate, intracellular acetate is at the cross-road of metabolic pathways and may contribute to lipogenesis and tricarboxylic acid (TCA) cycle.[18] Analysis of rabbit atherosclerotic arteries administered with ^{14}C-acetate has revealed that acetate contributes to both aqueous (e.g., glutamate) and fat-soluble (e.g., triglycerides and cholesterol esters) metabolites.[18,40,41] Our study demonstrated profound divergence of overall uptake of acetate by polarized murine macrophages and human atherosclerotic plaques. However, potential alterations in intra-cellular utilization of acetate by its differential fluxes through different pathways and the potential impact of these metabolic changes on macrophage biology and atherogenesis remained to be determined. Importantly, the dichotomy of IFN-γ + LPS (i.e., M1-like) and IL-4 (i.e. M2-like) stimulated macrophages fails to capture the profound and nuanced complexity of macrophage phenotypes and their unique metabolic and functional profiles.[42]

In this study, we took advantage of the higher spatial resolution of lower-energy β^- decay through ^{14}C-acetate autoradiography, in contrast to high-energy low-resolution β^+ by ^{11}C-acetate, to determine the histological distribution of acetate uptake within the vessel wall. The long half-life of ^{14}C-acetate was also compatible with the lengthy tissue processing steps required for micro-autoradiography, which would have been challenging for the short half-life of ^{11}C ($\sim$ 20 minutes). Although the use of ^{14}C-acetate eliminated the possibility of PET, the feasibility of in vivo detection of ^{11}C-acetate uptake in atherosclerosis has been previously demonstrated[17]; hence, our primary purpose was to determine the histological correlates of acetate uptake to unravel its association with plaque biology and eventually its clinical implications. Future clinical studies are needed to correlate in vivo ^{11}C-acetate uptake with molecular and histological markers of plaque vulnerability, like the macrophage burden, the abundance of different polarization states of macrophages, and pro/anti-inflammatory cytokine production, and disease outcome.

While acetate is a promising molecular imaging probe for atherosclerotic plaques,[17] certain limitations common to other immune-metabolic tracers, including low spatial resolution with respect to plaque size and low signal-to-background, remain roadblocks for translational application. Additionally, high ^{11}C-acetate uptake by metabolically active organs, particularly heart and liver, may limit its usefulness in imaging coronary artery disease.[17,43–45] ^{11}C-acetate PET may therefore be more suited for assessment of atherosclerosis in larger arteries, particularly carotid arteries, to predict and monitor response to conventional, e.g., statin, or emerging immunomodulatory therapies.

In summary, our data demonstrate that acetate uptake within the vessel wall primarily correlates with macrophage-rich atherosclerotic plaques. Moreover, classical proinflammatory polarization of macrophages and atherosclerotic plaques significantly reduces their uptake of acetate, while alternative activation upregulates the uptake. Together, these data suggest a potential link between the enhanced uptake of acetate and the induction of an inflammation-resolving state in atherosclerotic plaques. Further in vivo imaging studies are required to determine if ^{11}C-acetate PET, alone or in combination with other metabolic substrates, e.g., ^{18}F-FDG and ^{18}F-fluoroglutamine, may play a role in identifying vulnerable plaques and in monitoring the response to anti-inflammatory interventions, such as interleukin-1β blocking antibody, canakinumab.[46]

NEW KNOWLEDGE GAINED

Our results demonstrate that arterial uptake of acetate is mostly localized to macrophage-rich regions of atherosclerotic plaques compared to regions enriched in smooth muscle cells. Additionally, we showed that a profound divergence in acetate uptake distinguishes the classical (proinflammatory) and alternative (inflammation-resolving) polarization states of macrophages, induced by interferon-γ + lipopolysaccharide vs interleukin-4, respectively, in two different ex vivo models, i.e., cultured murine macrophages and human endarterectomy specimens. These data provide a new potential venue for in vivo immunometabolic characterization of plaques by non-invasive imaging.

Disclosures

The authors have no conflicts of interest to disclose.

References

1. Ketelhuth DFJ, Lutgens E, Back M, Binder CJ, Van den Bossche J, Daniel C, Dumitriu IE, Hoefer I, Libby P, O'Neill L, Weber C, Evans PC. Immunometabolism and atherosclerosis: Perspectives and clinical significance: A position Paper from the Working Group on Atherosclerosis and Vascular Biology of the European Society of Cardiology. Cardiovasc Res 2019;115:1385-92.
2. Koelwyn GJ, Corr EM, Erbay E, Moore KJ. Regulation of macrophage immunometabolism in atherosclerosis. Nat Immunol 2018;19:526-37.
3. Russell DG, Huang L, VanderVen BC. Immunometabolism at the interface between macrophages and pathogens. Nat Rev Immunol 2019;19:291-304.
4. Folco EJ, Sukhova GK, Quillard T, Libby P. Moderate hypoxia potentiates interleukin-1beta production in activated human macrophages. Circ Res 2014;115:875-83.
5. Folco EJ, Sheikine Y, Rocha VZ, Christen T, Shvartz E, Sukhova GK, Di Carli MF, Libby P. Hypoxia but not inflammation augments glucose uptake in human macrophages: Implications for imaging atherosclerosis with ^{18}fluorine-labeled 2-deoxy-D-glucose positron emission tomography. J Am Coll Cardiol 2011;58:603-14.
6. Marsch E, Sluimer JC, Daemen MJ. Hypoxia in atherosclerosis and inflammation. Curr Opin Lipidol 2013;24:393-400.
7. Marsch E, Theelen TL, Demandt JA, Jeurissen M, van Gink M, Verjans R, Janssen A, Cleutjens JP, Meex SJ, Donners MM, Haenen GR, Schalkwijk CG, Dubois LJ, Lambin P, Mallat Z, Gijbels MJ, Heemskerk JW, Fisher EA, Biessen EA, Janssen BJ, Daemen MJ, Sluimer JC. Reversal of hypoxia in murine atherosclerosis prevents necrotic core expansion by enhancing efferocytosis. Arterioscler Thromb Vasc Biol 2014;34:2545-53.
8. Tannahill GM, Curtis AM, Adamik J, Palsson-McDermott EM, McGettrick AF, Goel G, Frezza C, Bernard NJ, Kelly B, Foley NH, Zheng L, Gardet A, Tong Z, Jany SS, Corr SC, Haneklaus M, Caffrey BE, Pierce K, Walmsley S, Beasley FC, Cummins E, Nizet V, Whyte M, Taylor CT, Lin H, Masters SL, Gottlieb E, Kelly VP, Clish C, Auron PE, Xavier RJ, O'Neill LA. Succinate is an inflammatory signal that induces IL-1beta through HIF-1alpha. Nature 2013;496:238-42.
9. Tavakoli S, Downs K, Short JD, Nguyen HN, Lai Y, Jerabek PA, Goins B, Toczek J, Sadeghi MM, Asmis R. Characterization of macrophage polarization states using combined measurement of 2-deoxyglucose and glutamine accumulation: Implications for imaging of atherosclerosis. Arterioscler Thromb Vasc Biol 2017;37:1840-8.
10. Tavakoli S, Zamora D, Ullevig S, Asmis R. Bioenergetic profiles diverge during macrophage polarization: Implications for the interpretation of ^{18}F-FDG PET imaging of atherosclerosis. J Nucl Med 2013;54:1661-7.
11. Ngoi NYL, Eu JQ, Hirpara J, Wang L, Lim JSJ, Lee SC, Lim YC, Pervaiz S, Goh BC, Wong ALA. Targeting cell metabolism as cancer therapy. Antioxid Redox Signal 2020;32:285-308.
12. Luengo A, Gui DY, Vander Heiden MG. Targeting metabolism for cancer therapy. Cell Chem Biol 2017;24:1161-80.
13. Tavakoli S, Short JD, Downs K, Nguyen HN, Lai Y, Zhang W, Jerabek P, Goins B, Sadeghi MM, Asmis R. Differential regulation of macrophage glucose metabolism by macrophage colony-stimulating factor and granulocyte-macrophage colony-stimulating factor: Implications for $^{(18)}$F FDG PET imaging of vessel wall inflammation. Radiology 2017;283:87-97.
14. Al-Mashhadi RH, Tolbod LP, Bloch LO, Bjorklund MM, Nasr ZP, Al-Mashhadi Z, Winterdahl M, Frokiaer J, Falk E, Bentzon JF. $^{(18)}$fluorodeoxyglucose accumulation in arterial tissues determined by PET signal analysis. J Am Coll Cardiol 2019;74:1220-32.
15. Tavakoli S, Vashist A, Sadeghi MM. Molecular imaging of plaque vulnerability. J Nucl Cardiol 2014;21:1112-28; quiz 1129.
16. Tavakoli S. Technical considerations for quantification of $^{(18)}$F-FDG uptake in carotid atherosclerosis. J Nucl Cardiol 2019;26:894-8.
17. Derlin T, Habermann CR, Lengyel Z, Busch JD, Wisotzki C, Mester J, Pavics L. Feasibility of ^{11}C-acetate PET/CT for imaging of fatty acid synthesis in the atherosclerotic vessel wall. J Nucl Med 2011;52:1848-54.
18. Yamasaki K, Yamashita A, Zhao Y, Shimizu Y, Nishii R, Kawai K, Tamaki N, Zhao S, Asada Y, Kuge Y. In vitro uptake and metabolism of [$^{(14)}$C]acetate in rabbit atherosclerotic arteries: Biological basis for atherosclerosis imaging with [$^{(11)}$C]acetate. Nucl Med Biol 2018;56:21-5.
19. Dunphy MPS, Harding JJ, Venneti S, Zhang H, Burnazi EM, Bromberg J, Omuro AM, Hsieh JJ, Mellinghoff IK, Staton K, Pressl C, Beattie BJ, Zanzonico PB, Gerecitano JF, Kelsen DP, Weber W, Lyashchenko SK, Kung HF, Lewis JS. In vivo pet assay of tumor glutamine flux and metabolism: In-human trial of $^{(18)}$F-(2*S*, 4*R*)-4-fluoroglutamine. Radiology 2018;287:667-75.
20. Karanikas G, Beheshti M. $^{(1)(1)}$C-acetate pet/ct imaging: Physiologic uptake, variants, and pitfalls. PET Clin 2014;9:339-44.
21. Porenta G, Cherry S, Czernin J, Brunken R, Kuhle W, Hashimoto T, Schelbert HR. Noninvasive determination of myocardial blood flow, oxygen consumption and efficiency in normal humans by carbon-11 acetate positron emission tomography imaging. Eur J Nucl Med 1999;26:1465-74.
22. Zhang X, Goncalves R, Mosser DM. The isolation and characterization of murine macrophages. Curr Protoc Immunol 2008. https://doi.org/10.1002/0471142735.im1401s83.
23. Gomez D, Shankman LS, Nguyen AT, Owens GK. Detection of histone modifications at specific gene loci in single cells in histological sections. Nat Methods 2013;10:171-7.
24. Erbel C, Okuyucu D, Akhavanpoor M, Zhao L, Wangler S, Hakimi M, Doesch A, Dengler TJ, Katus HA, Gleissner CA. A human ex vivo atherosclerotic plaque model to study lesion biology. J Vis Exp 2014. https://doi.org/10.3791/50542.

25. Lebedeva A, Vorobyeva D, Vagida M, Ivanova O, Felker E, Fitzgerald W, Danilova N, Gontarenko V, Shpektor A, Vasilieva E, Margolis L. Ex vivo culture of human atherosclerotic plaques: A model to study immune cells in atherogenesis. Atherosclerosis 2017;267:90-8.
26. Balmer ML, Ma EH, Bantug GR, Grahlert J, Pfister S, Glatter T, Jauch A, Dimeloe S, Slack E, Dehio P, Krzyzaniak MA, King CG, Burgener AV, Fischer M, Develioglu L, Belle R, Recher M, Bonilla WV, Macpherson AJ, Hapfelmeier S, Jones RG, Hess C. Memory $CD8^{(+)}$ T cells require increased concentrations of acetate induced by stress for optimal function. Immunity 2016;44:1312-24.
27. Petersen C, Nielsen MD, Andersen ES, Basse AL, Isidor MS, Markussen LK, Viuff BM, Lambert IH, Hansen JB, Pedersen SF. MCT1 and MCT4 expression and lactate flux activity increase during white and brown adipogenesis and impact adipocyte metabolism. Sci Rep 2017;7:13101.
28. Jackson CL, Bennett MR, Biessen EA, Johnson JL, Krams R. Assessment of unstable atherosclerosis in mice. Arterioscler Thromb Vasc Biol 2007;27:714-20.
29. Rosenfeld ME, Polinsky P, Virmani R, Kauser K, Rubanyi G, Schwartz SM. Advanced atherosclerotic lesions in the innominate artery of the Apoe knockout mouse. Arterioscler Thromb Vasc Biol 2000;20:2587-92.
30. Johnson JL, Jackson CL. Atherosclerotic plaque rupture in the apolipoprotein e knockout mouse. Atherosclerosis 2001;154:399-406.
31. Sadeghi MM. $^{(18)}$F-FDG PET and vascular inflammation: Time to refine the paradigm? J Nucl Cardiol 2015;22:319-24.
32. Guillermier C, Doherty SP, Whitney AG, Babaev VR, Linton MF, Steinhauser ML, Brown JD. Imaging mass spectrometry reveals heterogeneity of proliferation and metabolism in atherosclerosis. JCI Insight 2019. https://doi.org/10.1172/jci.insight.128528.
33. Bose S, Ramesh V, Locasale JW. Acetate metabolism in physiology, cancer, and beyond. Trends Cell Biol 2019;29:695-703.
34. Vats D, Mukundan L, Odegaard JI, Zhang L, Smith KL, Morel CR, Wagner RA, Greaves DR, Murray PJ, Chawla A. Oxidative metabolism and PGC-1beta attenuate macrophage-mediated inflammation. Cell Metab 2006;4:13-24.
35. Tabas I, Bornfeldt KE. Intracellular and intercellular aspects of macrophage immunometabolism in atherosclerosis. Circ Res 2020;126:1209-27.
36. Tan Z, Xie N, Banerjee S, Cui H, Fu M, Thannickal VJ, Liu G. The monocarboxylate transporter 4 is required for glycolytic reprogramming and inflammatory response in macrophages. J Biol Chem 2015;290:46-55.
37. Puchalska P, Huang X, Martin SE, Han X, Patti GJ, Crawford PA. Isotope tracing untargeted metabolomics reveals macrophage polarization-state-specific metabolic coordination across intracellular compartments. iScience 2018;9:298-313.
38. Cumming BM, Addicott KW, Adamson JH, Steyn AJ. *Mycobacterium tuberculosis* induces decelerated bioenergetic metabolism in human macrophages. eLife 2018. https://doi.org/10.7554/eLife.39169.001.
39. Jha AK, Huang SC, Sergushichev A, Lampropoulou V, Ivanova Y, Loginicheva E, Chmielewski K, Stewart KM, Ashall J, Everts B, Pearce EJ, Driggers EM, Artyomov MN. Network integration of parallel metabolic and transcriptional data reveals metabolic modules that regulate macrophage polarization. Immunity 2015;42:419-30.
40. Howard CF Jr. Lipogenesis from glucose-2-14 C and acetate-1-14 C in aorta. J Lipid Res 1971;12:725-30.
41. Day AJ, Wilkinson GK. Incorporation of 14-C-labeled acetate into lipid by isolated foam cells and by atherosclerotic arterial intima. Circ Res 1967;21:593-600.
42. Nahrendorf M, Swirski FK. Abandoning M1/M2 for a network model of macrophage function. Circ Res 2016;119:414-7.
43. Armbrecht JJ, Buxton DB, Schelbert HR. Validation of [1-^{11}C]acetate as a tracer for noninvasive assessment of oxidative metabolism with positron emission tomography in normal, ischemic, postischemic, and hyperemic canine myocardium. Circulation 1990;81:1594-605.
44. Sun KT, Chen K, Huang SC, Buxton DB, Hansen HW, Kim AS, Siegel S, Choi Y, Muller P, Phelps ME, Schelbert HR. Compartment model for measuring myocardial oxygen consumption using [1-^{11}C]acetate. J Nucl Med 1997;38:459-66.
45. Nesterov SV, Turta O, Han C, Maki M, Lisinen I, Tuunanen H, Knuuti J. C-11 acetate has excellent reproducibility for quantification of myocardial oxidative metabolism. Eur Heart J Cardiovasc Imaging 2015;16:500-6.
46. Ridker PM, Everett BM, Thuren T, MacFadyen JG, Chang WH, Ballantyne C, Fonseca F, Nicolau J, Koenig W, Anker SD, Kastelein JJP, Cornel JH, Pais P, Pella D, Genest J, Cifkova R, Lorenzatti A, Forster T, Kobalava Z, Vida-Simiti L, Flather M, Shimokawa H, Ogawa H, Dellborg M, Rossi PRF, Troquay RPT, Libby P, Glynn RJ, Group CT. Antiinflammatory therapy with canakinumab for atherosclerotic disease. N Engl J Med 2017;377:1119-31.